arXiv:1903.11923v1 [astro-ph.SR] 28 Mar 2019

Comprehensive Determination of the *Hinode*/EIS Roll Angle

Gabriel Pelouze[1] · **Frédéric Auchère[1]** ·
Karine Bocchialini[1] · **Louise Harra[2]** ·
Deborah Baker[2] · **Harry P. Warren[3]** · **David
H. Brooks[4]** · **John T. Mariska[5]**

Abstract We present a new coalignment method for the *EUV Imaging Spectrometer* (EIS) on board the *Hinode* spacecraft. In addition to the pointing offset and spacecraft jitter, this method determines the roll angle of the instrument, which has never been systematically measured, and is therefore usually not corrected. The optimal pointing for EIS is computed by maximizing the cross-correlations of the Fe XII 195.119 Å line with images from the 193 Å band of the *Atmospheric Imaging Assembly* (AIA) on board the *Solar Dynamics Observatory* (SDO). By coaligning 3336 rasters with high signal-to-noise ratio, we estimate the rotation angle between EIS and AIA and explore the distribution of its values. We report an average value of $(-0.387 \pm 0.007)°$. We also provide a software implementation of this method that can be used to coalign any EIS raster.

Keywords: Hinode, EIS; Instrumental Effects; Instrumentation and Data Management; Spectrum, ultraviolet

✉ G. Pelouze
gabriel.pelouze@ias.u-psud.fr

[1]   Institut d'Astrophysique Spatiale, CNRS, Univ. Paris-Sud, Université Paris-Saclay, Bât. 121, 91405 Orsay cedex, France

[2]   Mullard Space Science Laboratory, University College London, Holmbury, St. Mary, Dorking, Surrey, KT22 9XF, UK

[3]   Space Science Division, Naval Research Laboratory, Washington, DC 20375, USA

[4]   College of Science, George Mason University, 4400 University Drive, Fairfax, VA 22030 USA

[5]   Department of Physics and Astronomy, George Mason University, 4400 University Drive, Fairfax, VA 22030, USA

1. Introduction

To analyze data from the *Extreme-ultraviolet (EUV) Imaging Spectrometer* (EIS: Culhane *et al.*, 2007) on board *Hinode* (Kosugi *et al.*, 2007), it is required to accurately correct the pointing of the instrument. This is usually done by registering (*i.e.* finding the geometrical transform between two images) EIS rasters with images from the *Atmospheric Imaging Assembly* (AIA: Lemen *et al.*, 2012) on board the *Solar Dynamics Observatory* (SDO: Pesnell, Thompson, and Chamberlin, 2012), or from the *Extreme-ultraviolet Imaging Telescope* (EIT: Delaboudinière *et al.*, 1995) on board the *Solar and Heliospheric Observatory* (SOHO: Domingo, Fleck, and Poland, 1995).

Registering EIS images with the reference instrument requires knowledge of two translations (the pointing offsets along the *X*- and *Y*-axis), a scaling factor (the ratio of the plate scales), and a rotation (the roll-angle difference in the plane of the sky). The roll angle is the most difficult parameter to determine.

The roll angles of the *X-Ray Telescope* (XRT: Golub *et al.*, 2007) and the *Solar Optical Telescope* (SOT: Tsuneta *et al.*, 2008), both on board *Hinode*, have been determined using transits of Mercury by Shimizu *et al.* (2007). The temporal evolution of the XRT roll angle was later measured by Yoshimura and McKenzie (2015), who used correlations with AIA and the *Helioseismic and Magnetic Imager* (HMI: Scherrer *et al.*, 2012) on board SDO. The authors find that this rotation angle changes periodically over one year with an amplitude of about $0.2°$. The roll angle of EIS, however, has never been determined, and is therefore not systematically accounted for. Indeed, very few studies report taking into account a rotation when coaligning EIS data (see, *e.g.*, Brooks, Warren, and Ugarte-Urra, 2012, who report doing so).

Furthermore, the spacecraft jitter randomly changes the spacecraft attitude by a few arcsec on all three axes and at each slit position during a raster scan (Shimizu *et al.*, 2007). This has a significant effect on the pointing offset, which can change by several pixels as a result. Therefore each slit position has to be coaligned independently from one another, along the *X*- and *Y*-directions. However, the effect of the jitter on the roll angle (*Z*-axis) is negligible, because it rotates the field of view (FOV) by a few arcsec in the plane of the sky (the same angle as around the *X*- and *Y*-axes). Over the largest EIS field of view ($512''$), a rotation of $10''$ would shift the observed structures by less than $0.02''$ (or 0.02 pixels) at the edge of the FOV. Because of this, we can search for an overall rotation angle common to all slit positions.

In Section 2, we present a new method to register EIS rasters with SDO/AIA images, that corrects the instrument roll and spacecraft jitter. In Section 3, we apply this method to get an accurate estimation of the roll angle between the spectrometer EIS and the imager AIA. In Section 4, we investigate the temporal dependency of this roll angle, and conclude that it is consistent with the findings of Yoshimura and McKenzie (2015) for XRT. Finally, we summarize our results and provide software to coalign EIS rasters with AIA in Section 5.

2. A New Method to Register EIS Rasters with AIA

2.1. Overview

We determine the pointing for an EIS raster by searching for the maximum cross-correlation between an Fe XII 195.119 Å intensity map and a synthetic raster built

from AIA 193 Å images. This synthetic raster simulates what would be seen by AIA if it acquired images by scanning each column at a time, as it is the case with EIS rasters. For efficiency, the Fe XII map is obtained by summing intensities between 194.969 and 195.269 Å from the level 1 EIS raster, which has been prepared with the routine eis_prep.pro from SolarSoft (Freeland and Handy, 2012). We verified that identical registration results are obtained when the intensities are computed using eis_auto_fit.pro, which fits Gaussians to the Fe XII 195.119 and 195.179 Å lines. The synthetic raster is obtained from a cube of level 1 AIA 193 Å images with a cadence of one minute, from which intensities are derived at the EIS spatial and temporal positions using bilinear interpolation. The synthetic raster is then degraded to the resolution of EIS by convolving it with a gaussian PSF of 3″ FWHM (Del Zanna, O'Dwyer, and Mason, 2011; Young *et al.*, 2013). In order for the AIA data to be as close as possible to what would be observed by EIS, we use different synthetic rasters when computing the cross-correlation map, which are generated for each sampled value of offset and rotation. Using synthetic rasters instead of a single AIA image is necessary because structures on the Sun may change significantly during the acquisition of the EIS raster, which can take up to several hours. We use the plate scale value of 1″ pixel^{-1} from the EIS headers. Although this value slightly differs from the $(1.002 \pm 0.016)''$ pixel^{-1} reported by Hara (2008), comparison between aligned EIS and AIA images shows no significant deformation of the structures that could be caused by an incorrect plate scale.

Searching for the global maximum cross-correlation in one run would require excessive computation time because the parameter space to explore is very large. Therefore we perform the correction in three sequential steps to save time: 1. determine and correct the average translation; 2. determine and correct the roll angle; 3. correct the jitter by coaligning each slit position independently. At step 1, we search for a translation that can be as large as the raster field of view. At step 2, we simultaneously search for rolls around the center of the field of view with angles between -3 and $3°$, along with a smaller translation (between -10 and $10''$ along the X-axis, and -5 and $5''$ along the Y-axis). At step 3 we search for translations of each slit position (*i.e.* each column of the raster), between -20 and $20''$ along both axes. These search limits were chosen by computing the cross-correlation over a wider range of offsets for about a hundred of rasters, and looking at the distributions of the maximum position.

2.2. Performance

For rasters with sufficient SNR (exposure times greater than 15 seconds with the 1″ slit for on-disk observations), our method can efficiently correct the visible deformation of the structures due to the instrument rotation and satellite jitter. We present registration results for raster eis_l0_20140810_042212, which corresponds to the observation of the active region NOAA 12135 on 10 August 2014 starting from 04:22:12 UT. This raster features an exposure time of 15 seconds at each position of the 1″ slit, a scan step of 2″, and a field of view of $480'' \times 512''$. The field of view of this raster is shown in Figure 1. The registration gives an offset of $(17.0'', 10.6'')$, a roll angle of $-0.78°$, and the slit offsets that are plotted in Figure 2. For this raster, the dispersion of the slit offset values is of about 2″ to 3″, and the offset along the Y-axis shows additional large scale variations of about 15″. Other rasters have a similar dispersion, but do not share any large-scale variation pattern. The dispersion and absolute values of the

slit offset don't appear to be correlated with the *Hinode* eclipse season, during which the Sun is periodically eclipsed by the upper Earth atmosphere, causing larger average pointing offsets (Mariska, 2016; Yoshimura and McKenzie, 2015). In order to obtain the corrected coordinates, these offsets are added to the original EIS coordinates, and the image is rotated clockwise.
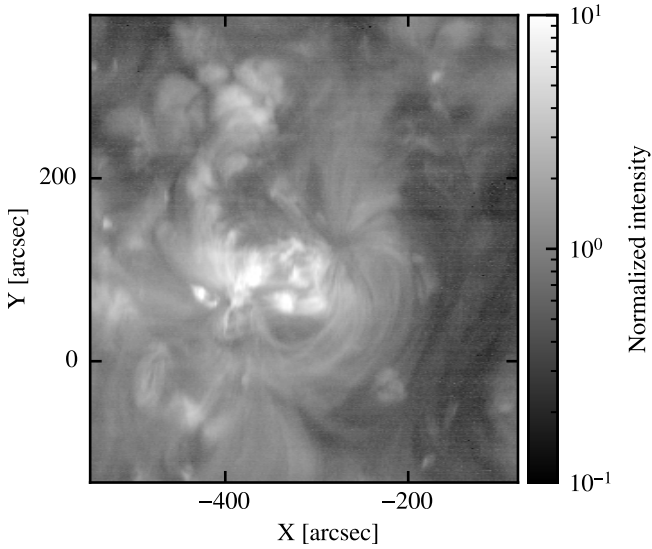
Figure 1. Map of the Fe XII 195.119 Å line emission for raster eis_l0_20140810_042212. The intensity is normalized to its standard deviation over the field of view, and the axes are labelled with the original EIS pointing.
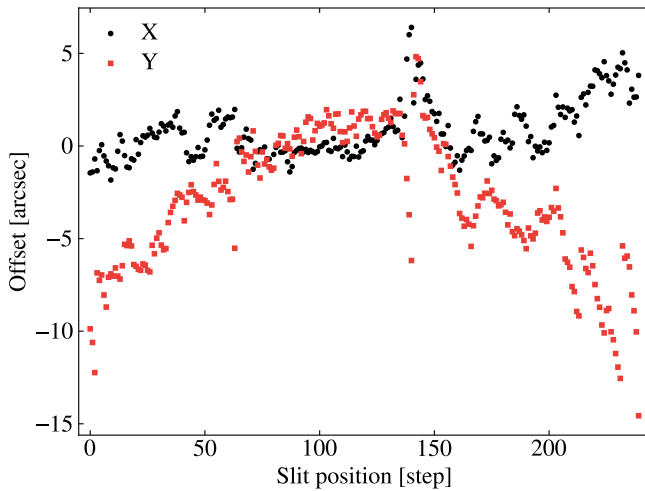
Figure 2. Slit offsets obtained when correcting the jitter for raster eis_l0_20140810_042212. Black dots represent offsets along the *X*-direction, while red squares represent offsets along the *Y*-direction.

In Figure 3, we show the difference between aligned EIS and AIA intensity maps, which have been normalized to their respective standard deviations. An animated version of this figure is also available as an electronic supplementary material, which allows us to better visualize the rotation and deformations in the field of view by showing the EIS and AIA intensity maps alternately. The visible variation between structures observed in both images is quantified by the root mean square (RMS) of this normalized intensity difference. The original data have a RMS of 0.769, which decreases to 0.177 after the registration is performed. In addition to alignment errors, the residuals are affected by differences in solar structures when observed in the EIS Fe XII 195.119 Å line, or the AIA 193 Å channel.
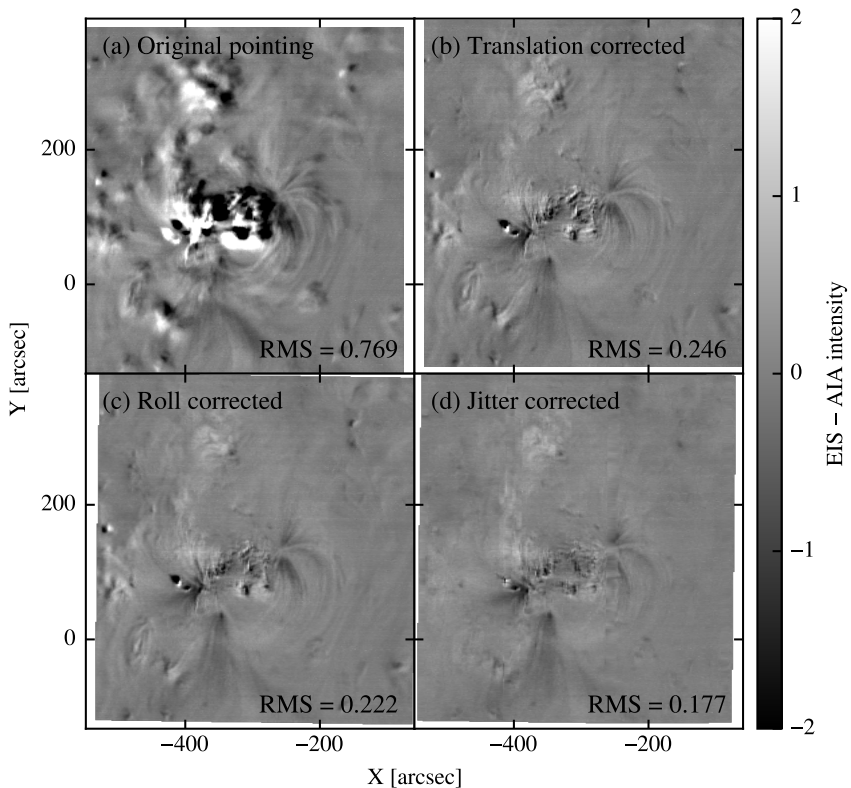
Figure 3. Registration result for raster eis_l0_20140810_042212. Each panel contains a map of the difference between normalized EIS and AIA intensities at each step of the registration: *(a)* original EIS pointing, *(b)* average translation corrected, *(c)* roll corrected, and *(d)* jitter corrected. The root mean square shown on each panels quantifies the difference between structures observed in EIS and AIA. An animated version of this figure is available as an electronic supplementary material, where the EIS and AIA intensity maps are shown alternately; this allows us to better visualize the rotation and deformations of the structures.

We performed additional testing to validate the method. First, we correct the jitter before correcting the roll angle (*i.e.* swapping registration steps 2 and 3). As shown in Figure 4, this achieves worse results with a rotation still visible in the animated version, and a final RMS of only 0.182. We also apply a second roll correction after correcting the jitter. This does not improve the pointing and results in the same final RMS of 0.177. Finally, we verify whether the measured roll angle may be caused by tilts between the internal components of EIS. The *slit tilt* is a known angle between the slits and the EIS detectors, which slants spectral lines on the detector (Young, 2010). On the short wavelength (SW) detector, lines are rotated by 0.03° with the 1″ slit, and by 0.3° with the 2″ slit. While this can significantly modify measured velocities, it should have no influence on the pointing. However, the pointing would be affected by an angle between the slits and the tilt axis of the mirror, which defines the direction along which a raster is scanned. This would result in a sheared image, meaning that each slit position appears to be rotated by a given angle relatively to the scanning direction. We aligned raster eis_l0_20140810_042212 by replacing the search for a roll angle (step 2) with the search for a shear transform. Because this could not correct the visible rotation of the field of view, we rule out the presence of a rotation between the slits and the tilt-mirror mechanism as the source of the observed roll.

From these tests, we conclude that three registration steps are required in order to accurately register EIS maps with AIA, and that the best results are achieved when they are applied in the following order : translation, rotation, and jitter.
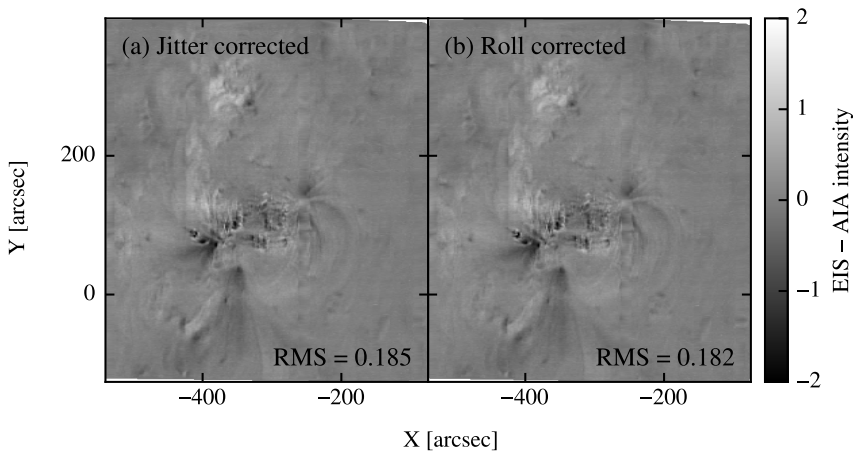
Figure 4. Registration result for raster eis_l0_20140810_042212, swapping steps 2 and 3: *(a)* jitter corrected, and *(b)* roll corrected. (See Figure 3 for the reference alignment.) An animated version of this figure is available as an electronic supplementary material.

3. Results: EIS Roll Angle

To accurately measure the roll angle between EIS and *Hinode* we correlate a large number of rasters with AIA. We query the EIS database (sdc.uio.no) for rasters recorded

between 13 May 2010 and 4 September 2018 that match the following criteria: the center of the raster is on-disk, the field of view is wider than $200''$, the raster uses either the $1''$ or the $2''$ slit, and the exposure time is longer than 15 seconds. The query returns 3856 rasters that we process with the method described in Section 2.

Most of the rasters are successfully registered, which results in 3707 measurements of the roll angle between EIS and AIA. 80 of the failed measurements were caused by bad initial EIS pointing (file headers indicate a raster center far outside the disk), 48 by missing or corrupted AIA data, and 21 by errors during the EIS data preparation or too many missing pixels in the resulting raster. In order to discard bad registrations, we remove 10 % of the alignment results for which the RMS of the EIS and AIA intensity difference is the largest. The histogram of the $N = 3336$ remaining roll-angle values is shown in Figure 5. This distribution can be approximated by a Gaussian centered at $\theta_0 = -0.387°$, and with a standard deviation of $\sigma_\theta = 0.399°$. The uncertainty on θ_0 is given by $\sigma_\theta / \sqrt{N}$. Therefore, we estimate the average roll angle between EIS and AIA to be $(-0.387 \pm 0.007)°$. The dispersion σ_θ can be due to a combination of measurement errors, and/or true variations of the roll angle. For this reason, the uncertainty on the roll angle for an arbitrary raster is larger than $0.007°$. Thus to coalign an EIS raster with an AIA image, the EIS raster must be rotated by $-0.387°$, *i.e.* a clockwise rotation.
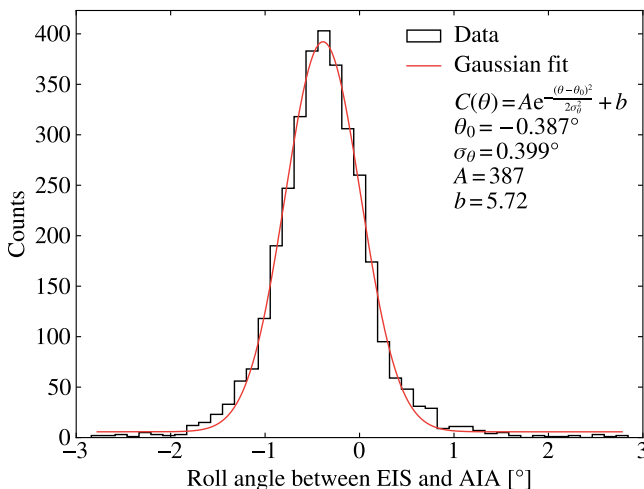
Figure 5. Histogram of the roll angle between EIS and AIA measured on 3336 rasters between 2010 and 2018. The red line is a Gaussian that fits the histogram, with a center at $-0.387°$, and a standard deviation of $0.399°$.

4. Discussion

In order to understand the distribution of roll-angle values, we investigate how they depend on several parameters, such as exposure time, field-of-view size, orbit phase, raster duration, scan step, and slit width. We find that none of these parameters significantly affect the roll angle. We also search for structures in the time series of roll-angle values, which is shown in Figure 6. While there appears to be no secular evolution of the average values, we also search for periodic variations. To that end, we estimate the power

spectral density (PSD) of the roll-angle time series using a Lomb–Scargle periodogram (Lomb, 1976; Scargle, 1982) shown in Figure 7. To model the noise, we fit the PSD with a power law $\sigma(\nu) = A\nu^s$, which yields $A = 0.013$, and $s = -0.35$. The probability that at least one peak has a power greater than $m\sigma(\nu)$ is $P(m) = 1 - (1 - e^{-m})^{N_i}$, where N_i is the number of independent frequencies (Scargle, 1982; Gabriel *et al.*, 2002; Auchère *et al.*, 2016). However, estimating the number of independent frequencies for unevenly spaced data is difficult. In our case, the rasters are sometimes closely clumped in time, which can significantly reduce the number of independent frequencies (relatively to the case of evenly spaced measurements), and therefore lower confidence levels (Horne and Baliunas, 1986). We estimate an upper bound for the confidence levels by assuming that the samples are regularly spaced, which implies that $N_i = N$. The periodogram reveals two peaks above the 99 % confidence level: one with a period of one year, and the other with a period of 7.6 days.
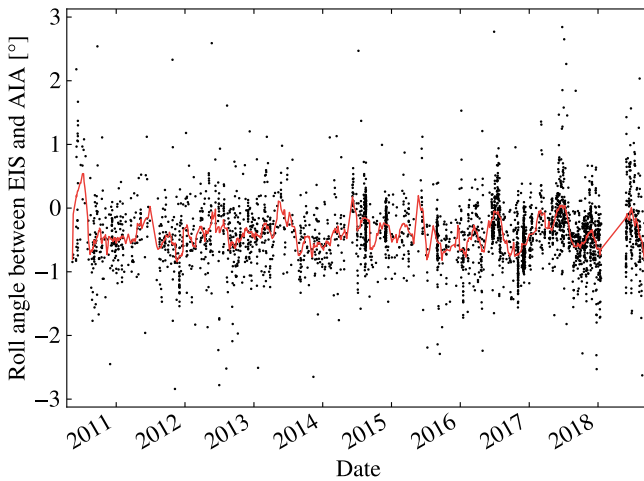
Figure 6. Time series of the roll angle between EIS and AIA measured on 3336 rasters between 2010 and 2018. Individual measurements are plotted as black dots, and a 20-day boxcar running average is shown as a red line.

The first peak is consistent with the results of Yoshimura and McKenzie (2015), who find that the roll angle between XRT and AIA or HMI changes periodically over one year, with an amplitude of about 0.2° and an average of +0.34°. They also find that the roll angle is largest at the end of July each year, and smallest at the end of January. While the one-year variation is not visible directly in our raw time series, applying a 20-day boxcar running average, shown in Figure 6, reveals that the roll angle between EIS and AIA is also at its maximum around July. The fact that the roll angles between EIS and AIA (this study), and between XRT and AIA or HMI (Yoshimura and McKenzie, 2015) display similar variations but have different averages suggests that the constant part comes from alignment offsets of the instruments with respect to *Hinode*, while the variations come from the behaviour of the spacecrafts (*Hinode* and/or SDO), regardless of the instruments.

Obtaining true solar coordinates for EIS should require no additional step once it is registered with AIA, because we use the pointing information present in the AIA
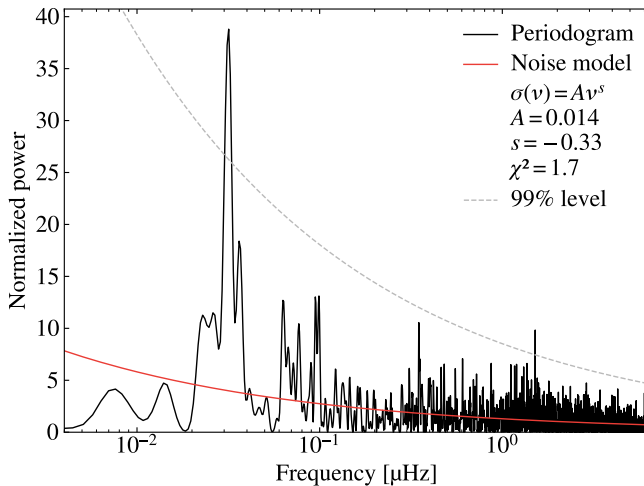
Figure 7. Lomb–Scargle periodogram of the time series of the roll angle between EIS and AIA measured on 3336 rasters between 2010 and 2018. The power-law noise model is shown as a solid red line, and the 99 % confidence level is shown as a gray dashed line.

level 1 image headers, which are corrected for plate scale, telescope coalignment, and roll relatively to the solar North (Lemen *et al.*, 2012; Boerner *et al.*, 2012).

5. Conclusion

We developed a new method to register EIS rasters with SDO/AIA, which can determine and correct the pointing offsets and the roll angle between the two instruments, as well as the *Hinode* jitter. By applying this method to 3336 rasters recorded between May 2010 and September 2018, we were able to measure the average roll angle between EIS and AIA to a value of $(-0.387 \pm 0.007)°$. Such a rotation shifts the structures by $3.5''$ over $512''$, which is the size of large EIS rasters. We also found evidence for a time dependency of this roll angle, which results in a standard deviation of $0.399°$. For this reason, we recommend that the roll angle is determined for each raster whenever possible.

The implementation of our registration method is provided as a Python package, which can be found at github.com/gpelouze/eis_pointing. This tool can be used to coalign EIS rasters with AIA images when precise spatial information is required. While correcting the jitter requires high SNR (typically 15 second exposure time with the $1''$ slit for on-disk observations), the determination of the pointing offset and of the roll angle should work on most rasters.

Disclosure of Potential Conflicts of Interest   The authors declare that they have no conflicts of interest.

References

Astropy Collaboration, Robitaille, T.P., Tollerud, E.J., Greenfield, P., Droettboom, M., Bray, E., Aldcroft, T., Davis, M., Ginsburg, A., Price-Whelan, A.M., Kerzendorf, W.E., Conley, A., Crighton, N., Barbary, K., Muna, D., Ferguson, H., Grollier, F., Parikh, M.M., Nair, P.H., Unther, H.M., Deil, C., Woillez, J., Conseil, S., Kramer, R., Turner, J.E.H., Singer, L., Fox, R., Weaver, B.A., Zabalza, V., Edwards, Z.I., Azalee Bostroem, K., Burke, D.J., Casey, A.R., Crawford, S.M., Dencheva, N., Ely, J., Jenness, T., Labrie, K., Lim, P.L., Pierfederici, F., Pontzen, A., Ptak, A., Refsdal, B., Servillat, M., Streicher, O.: 2013, Astropy: A community Python package for astronomy. *Astron. Astrophys.* **558**, A33. DOI. ADS.

Astropy Collaboration, Price-Whelan, A.M., Sipőcz, B.M., Günther, H.M., Lim, P.L., Crawford, S.M., Conseil, S., Shupe, D.L., Craig, M.W., Dencheva, N., Ginsburg, A., VanderPlas, J.T., Bradley, L.D., Pérez-Suárez, D., de Val-Borro, M., Aldcroft, T.L., Cruz, K.L., Robitaille, T.P., Tollerud, E.J., Ardelean, C., Babej, T., Bach, Y.P., Bachetti, M., Bakanov, A.V., Bamford, S.P., Barentsen, G., Barmby, P., Baumbach, A., Berry, K.L., Biscani, F., Boquien, M., Bostroem, K.A., Bouma, L.G., Brammer, G.B., Bray, E.M., Breytenbach, H., Buddelmeijer, H., Burke, D.J., Calderone, G., Cano Rodríguez, J.L., Cara, M., Cardoso, J.V.M., Cheedella, S., Copin, Y., Corrales, L., Crichton, D., D'Avella, D., Deil, C., Depagne, É., Dietrich, J.P., Donath, A., Droettboom, M., Earl, N., Erben, T., Fabbro, S., Ferreira, L.A., Finethy, T., Fox, R.T., Garrison, L.H., Gibbons, S.L.J., Goldstein, D.A., Gommers, R., Greco, J.P., Greenfield, P., Groener, A.M., Grollier, F., Hagen, A., Hirst, P., Homeier, D., Horton, A.J., Hosseinzadeh, G., Hu, L., Hunkeler, J.S., Ivezić, Ž., Jain, A., Jenness, T., Kanarek, G., Kendrew, S., Kern, N.S., Kerzendorf, W.E., Khvalko, A., King, J., Kirkby, D., Kulkarni, A.M., Kumar, A., Lee, A., Lenz, D., Littlefair, S.P., Ma, Z., Macleod, D.M., Mastropietro, M., McCully, C., Montagnac, S., Morris, B.M., Mueller, M., Mumford, S.J., Muna, D., Murphy, N.A., Nelson, S., Nguyen, G.H., Ninan, J.P., Nöthe, M., Ogaz, S., Oh, S., Parejko, J.K., Parley, N., Pascual, S., Patil, R., Patil, A.A., Plunkett, A.L., Prochaska, J.X., Rastogi, T., Reddy Janga, V., Sabater, J., Sakurikar, P., Seifert, M., Sherbert, L.E., Sherwood-Taylor, H., Shih, A.Y., Sick, J., Silbiger, M.T., Singanamalla, S., Singer, L.P., Sladen, P.H., Sooley, K.A., Sornarajah, S., Streicher, O., Teuben, P., Thomas, S.W., Tremblay, G.R., Turner, J.E.H., Terrón, V., van Kerkwijk, M.H., de la Vega, A., Watkins, L.L., Weaver, B.A., Whitmore, J.B., Woillez, J., Zabalza, V., Astropy Contributors: 2018, The Astropy Project: Building an Open-science Project and Status of the v2.0 Core Package. *Astron. J.* **156**, 123. DOI. ADS.

Auchère, F., Froment, C., Bocchialini, K., Buchlin, E., Solomon, J.: 2016, On the Fourier and Wavelet Analysis of Coronal Time Series. *Astrophys. J.* **825**, 110. DOI. ADS.

Boerner, P., Edwards, C., Lemen, J., Rausch, A., Schrijver, C., Shine, R., Shing, L., Stern, R., Tarbell, T., Title, A., Wolfson, C.J., Soufli, R., Spiller, E., Gullikson, E., McKenzie, D., Windt, D., Golub, L., Podgorski, W., Testa, P., Weber, M.: 2012, Initial Calibration of the Atmospheric Imaging Assembly (AIA) on the Solar Dynamics Observatory (SDO). *Solar Phys.* **275**(1-2), 41. DOI. ADS.

Brooks, D.H., Warren, H.P., Ugarte-Urra, I.: 2012, Solar Coronal Loops Resolved by Hinode and the Solar Dynamics Observatory. *Astrophys. J.* **755**(2), L33. DOI. ADS.

Culhane, J.L., Harra, L.K., James, A.M., Al-Janabi, K., Bradley, L.J., Chaudry, R.A., Rees, K., Tandy, J.A., Thomas, P., Whillock, M.C.R., Winter, B., Doschek, G.A., Korendyke, C.M., Brown, C.M., Myers, S., Mariska, J., Seely, J., Lang, J., Kent, B.J., Shaughnessy, B.M., Young, P.R., Simnett, G.M., Castelli, C.M., Mahmoud, S., Mapson-Menard, H., Probyn, B.J., Thomas, R.J., Davila, J., Dere, K., Windt, D., Shea, J., Hagood, R., Moye, R., Hara, H., Watanabe, T., Matsuzaki, K., Kosugi, T., Hansteen, V., Wikstol, Ø.: 2007, The EUV Imaging Spectrometer for Hinode. *Solar Phys.* **243**, 19. DOI. ADS.

Del Zanna, G., O'Dwyer, B., Mason, H.E.: 2011, SDO AIA and Hinode EIS observations of "warm" loops. *Astron. Astrophys.* **535**, A46. DOI. ADS.

Delaboudinière, J.-P., Artzner, G.E., Brunaud, J., Gabriel, A.H., Hochedez, J.F., Millier, F., Song, X.Y., Au, B., Dere, K.P., Howard, R.A., Kreplin, R., Michels, D.J., Moses, J.D., Defise, J.M., Jamar, C., Rochus, P., Chauvineau, J.P., Marioge, J.P., Catura, R.C., Lemen, J.R., Shing, L., Stern, R.A., Gurman, J.B., Neupert, W.M., Maucherat, A., Clette, F., Cugnon, P., van Dessel, E.L.: 1995, EIT: Extreme-Ultraviolet Imaging Telescope for the SOHO Mission. *Solar Phys.* **162**, 291. DOI. ADS.

Domingo, V., Fleck, B., Poland, A.I.: 1995, The SOHO Mission: An Overview. *Solar Phys.* **162**, 1. DOI. ADS.

Freeland, S.L., Handy, B.N.: 2012, SolarSoft: Programming and data analysis environment for solar physics. *Astrophysics Source Code Library*, ascl:1208.013. ADS.

Gabriel, A.H., Baudin, F., Boumier, P., García, R.A., Turck-Chièze, S., Appourchaux, T., Bertello, L., Berthomieu, G., Charra, J., Gough, D.O., Pallé, P.L., Provost, J., Renaud, C., Robillot, J.-M., Roca Cortés, T., Thiery, S., Ulrich, R.K.: 2002, A search for solar g modes in the GOLF data. *Astron. Astrophys.* **390**, 1119. DOI. ADS.

Golub, L., Deluca, E., Austin, G., Bookbinder, J., Caldwell, D., Cheimets, P., Cirtain, J., Cosmo, M., Reid, P., Sette, A., Weber, M., Sakao, T., Kano, R., Shibasaki, K., Hara, H., Tsuneta, S., Kumagai, K., Tamura, T., Shimojo, M., McCracken, J., Carpenter, J., Haight, H., Siler, R., Wright, E., Tucker, J., Rutledge, H., Barbera, M., Peres, G., Varisco, S.: 2007, The X-Ray Telescope (XRT) for the Hinode Mission. *Solar Phys.* **243**, 63. DOI. ADS.

Hara, H.: 2008, Overview of EIS Performance. In: Matthews, S.A., Davis, J.M., Harra, L.K. (eds.) *First Results From Hinode*, *Astronomical Society of the Pacific Conference Series* **397**, 11. ADS.

Horne, J.H., Baliunas, S.L.: 1986, A Prescription for Period Analysis of Unevenly Sampled Time Series. *Astrophys. J.* **302**, 757. DOI. ADS.

Kosugi, T., Matsuzaki, K., Sakao, T., Shimizu, T., Sone, Y., Tachikawa, S., Hashimoto, T., Minesugi, K., Ohnishi, A., Yamada, T., Tsuneta, S., Hara, H., Ichimoto, K., Suematsu, Y., Shimojo, M., Watanabe, T., Shimada, S., Davis, J.M., Hill, L.D., Owens, J.K., Title, A.M., Culhane, J.L., Harra, L.K., Doschek, G.A., Golub, L.: 2007, The Hinode (Solar-B) Mission: An Overview. *Solar Phys.* **243**, 3. DOI. ADS.

Lemen, J.R., Title, A.M., Akin, D.J., Boerner, P.F., Chou, C., Drake, J.F., Duncan, D.W., Edwards, C.G., Friedlaender, F.M., Heyman, G.F., Hurlburt, N.E., Katz, N.L., Kushner, G.D., Levay, M., Lindgren, R.W., Mathur, D.P., McFeaters, E.L., Mitchell, S., Rehse, R.A., Schrijver, C.J., Springer, L.A., Stern, R.A., Tarbell, T.D., Wuelser, J.-P., Wolfson, C.J., Yanari, C., Bookbinder, J.A., Cheimets, P.N., Caldwell, D., Deluca, E.E., Gates, R., Golub, L., Park, S., Podgorski, W.A., Bush, R.I., Scherrer, P.H., Gummin, M.A., Smith, P., Auker, G., Jerram, P., Pool, P., Soufli, R., Windt, D.L., Beardsley, S., Clapp, M., Lang, J., Waltham, N.: 2012, The Atmospheric Imaging Assembly (AIA) on the Solar Dynamics Observatory (SDO). *Solar Phys.* **275**, 17. DOI. ADS.

Lomb, N.R.: 1976, Least-Squares Frequency Analysis of Unequally Spaced Data. *Astrophys. Space Sci.* **39**(2), 447. DOI. ADS.

Mariska, J.: 2016, EIS Software Note No. 20: EIS/AIA Coalignment. In: *SolarSoft Documentation*.

Pesnell, W.D., Thompson, B.J., Chamberlin, P.C.: 2012, The Solar Dynamics Observatory (SDO). *Solar Phys.* **275**, 3. DOI. ADS.

Scargle, J.D.: 1982, Studies in astronomical time series analysis. II. Statistical aspects of spectral analysis of unevenly spaced data. *Astrophys. J.* **263**, 835. DOI. ADS.

Scherrer, P.H., Schou, J., Bush, R.I., Kosovichev, A.G., Bogart, R.S., Hoeksema, J.T., Liu, Y., Duvall, T.L., Zhao, J., Title, A.M., Schrijver, C.J., Tarbell, T.D., Tomczyk, S.: 2012, The Helioseismic and Magnetic Imager (HMI) Investigation for the Solar Dynamics Observatory (SDO). *Solar Phys.* **275**, 207. DOI. ADS.

Shimizu, T., Katsukawa, Y., Matsuzaki, K., Ichimoto, K., Kano, R., Deluca, E.E., Lundquist, L.L., Weber, M., Tarbell, T.D., Shine, R.A., Sôma, M., Tsuneta, S., Sakao, T., Minesugi, K.: 2007, Hinode Calibration for Precise Image Co-Alignment between SOT and XRT (2006 November-2007 April). *Pub. Astron. Soc. Japan* **59**, S845. DOI. ADS.

Tsuneta, S., Ichimoto, K., Katsukawa, Y., Nagata, S., Otsubo, M., Shimizu, T., Suematsu, Y., Nakagiri, M., Noguchi, M., Tarbell, T., Title, A., Shine, R., Rosenberg, W., Hoffmann, C., Jurcevich, B., Kushner, G., Levay, M., Lites, B., Elmore, D., Matsushita, T., Kawaguchi, N., Saito, H., Mikami, I., Hill, L.D., Owens, J.K.: 2008, The Solar Optical Telescope for the Hinode Mission: An Overview. *Solar Phys.* **249**, 167. DOI. ADS.

Yoshimura, K., McKenzie, D.E.: 2015, Calibration of Hinode/XRT for Coalignment. *Solar Phys.* **290**(8), 2355. DOI. ADS.

Young, P.: 2010, EIS Software Note No. 4: The EIS Slit Tilts. In: *SolarSoft Documentation*.

Young, P.R., Doschek, G.A., Warren, H.P., Hara, H.: 2013, Properties of a Solar Flare Kernel Observed by Hinode and SDO. *Astrophys. J.* **766**(2), 127. DOI. ADS.